Journal of Thermal Analysis and Calorimetry (2022) 147:10371–10381
https://doi.org/10.1007/s10973-022-11302-x

Study of structural, thermal and piezoelectric properties of polyvinylidene fluoride –$BaZrO_3$ nanocomposites

Rohan Sagar[1] · M. S. Gaur[1] · Rajesh Kumar Raghav[1]

Received: 7 June 2021 / Accepted: 1 March 2022 / Published online: 4 April 2022

Abstract

The thin film of nanocomposites was prepared by solution casting methods and characterized by UV–Vis spectra, Raman spectra and scanning electron microscopy (SEM). The optical band gap was determined by Tau plots. The band gap of PVDF was determined with and without $BaZrO_3$ nanoparticles. It could be seen that the band gap decreases from 4.98 to 3.32 eV in the presence of $BaZrO_3$ nanoparticles in PVDF matrix. The Raman study identifies the interacting species with PVDF due to structural change by the addition of $BaZrO_3$ nanoparticles. This helps to understand the potential of new nanocomposites. The structural changes were analyzed by crystallinity, nature of bonds, phase transition from G to B-phase, etc. SEM images represent the change in spherulitic morphology of PVDF by incorporation of $BaZrO_3$ nanoparticles. SEM images are presented the aggregation of $BaZrO_3$ nanoparticles in PVDF matrix causes the generation of larger particles in PVDF chain. DSC supports the crystallization of PVDF nanocomposites upon heating due to the rearrangement of PVDF structure in the presence of $BaZrO_3$ nanoparticles. It is observed that $BaZrO_3$ nanoparticles enrich the structural, thermal and piezoelectric properties due to the change in spherulitic morphology, which creates a large number of micro- to nano-sized pores, increases the β-phase content of the PVDF.

Keywords PVDF · $BaZrO_3$ · Raman · SEM · Piezoelectric · DSC

Introduction

There are potential applications of polyvinylidene fluoride (PVDF) nanocomposites in the area of optoelectronics and piezoelectric devices [1–3]. PVDF is one of the first flexible and efficient electromechanical materials. The polar nature is due to the positive charge on hydrogen and the negative charge in fluorine atoms. PVDF is an excellent piezoelectric polymer gaining importance amongst various polymers [4–8].

The previous studies proved that the PVDF is one of the most electroactive polymers mainly due to the presence of β- and γ-phases. The role of β- and γ-phases promoted its applications in the field of sensors, energy storage devices, etc. Moreover, its easy processing can improve the structural, electrical and mechanical properties [9–16]. The increase of β-phase in PVDF is subjected to the processing conditions. The solution casting, spin coating, and bland technique are the most important processing methods. It has been observed that the incorporation of inorganic nanoparticles is one of the strategic parts to improve the functional properties of polymers. Currently, nanofiller like ceramic nanoparticles are popular to improve the β-phase. There are some of the important nanofillers (i.e., CuO, NiO, Pt, $BaZrO_3$, $BaTiO_3$, etc.) that are considered to enhance β-phase of PVDF [17–24].

The combinations of polymers and ceramic nanofillers have received significant attention due to their excellent properties, which are suitable for flexible electronic devices such as embedded capacitors system, multilayer capacitors, field-effect transistors, piezo and pyroelectric sensors [25]. There are five crystalline phases of PVDF. Out of these, only electroactive β-phase is highly demanded because it exhibits a high dipole moment. This makes the polymer of high dielectric constant, high piezo and pyroelectric coefficients [26].

✉ M. S. Gaur
mulayamgaur@rediffmail.com

[1] Department of Physics, Hindustan College of Science and Technology, Farah, Mathura, U.P 281122, India affiliated to Dr. A.P.J. Abdul Kalama Technical University, Lucknow, U.P 226031, India

Barium zirconate is a ferroelectric ceramic material that possesses outstanding electroactive properties [27, 28]. Its crystalline structure is fcc type. Its structure consists of tetravalent ions at the centre of the cube and divalent ions at the top corner. However, O^{2-} ions are placed at the centre of each face.

The -OH groups of $BaZrO_3$ nanoparticles, as mixed with PVDF, provide strong hydrogen bonding sites and increase the electroactive β-phase. There are several questions regarding piezoelectric, dielectric, thermal properties, etc., of these nanocomposites that are unanswered. Understanding of the microscopic mechanisms of polarization reversal in PVDF nanocomposites is a critical issue amongst researchers.

The wide variety of PVDF nanocomposites have been developed with improved thermal, mechanical, and excellent barrier properties [29–31]. However, developing the PVDF nanocomposites for prolonged service at high temperatures is still a challenge.

The melting temperature of PVDF of different phases is in the range of 167–172 °C. The DSC is used to determine several parameters of material such as glass transition temperature, melting temperature, percentage crystallinity, and other thermal properties; however, it is unable to distinguish different phases of PVDF clearly. For this purpose FTIR, X-ray and Raman spectra are used [32–37].

Currently, nanocomposites play a very important role in the field of flexible electronic industries due to the simple architecting of nanofiller in the polymer matrix and their uncommon properties. The less number of publications of PVDF-$BaZrO_3$ nanocomposites have been found in literature. Therefore, in this work, the possibility of preparing $BaZrO_3$ embedded PVDF with different concentrations is demonstrated. In the present work, the optical, structural, electroactive and thermal properties of PVDF-$BaZrO_3$ nanocomposites were studied by UV–Vis spectroscopy, Raman spectroscopy and SEM–EDX spectra, P-E loop and DSC techniques. This research would help us better understand the effect of $BaZrO_3$ on the structure and properties of PVDF nanocomposites.

Experimental

Materials

PVDF was procured from Redox (India). The 64.03 and 1.78 g cm^{-3} are molecular weight and molecular density of PVDF. The N, N, dimethylformamide (DMF) was procured from Merck India Ltd. The barium zirconate ($BaZrO_3$) nanoparticles of size less than 100 nm were procured from Sigma Aldrich. All materials are used as obtained without any further processing for the preparation of nanocomposites. The material properties are presented in Table 1.

Table 1 Properties of PVDF and $BaZrO_3$ nanoparticles

Material	Density/g cm^{-3}	Particle size/nm	Specific surface area/ m^2g^{-1}	Purity/%
PVDF	1.78	100	3.76–6.61	99
$BaZrO_3$	5.96	25–50	3.5–11.2	98

Method

In this method, the PVDF is dissolved in N, N, dimethylformamide (DMF). The $BaZrO_3$ nanoparticles have higher chemical compatibility with PVDF due to the existence of hydroxyl groups onto the surface of $BaZrO_3$ nanoparticles. The $BaZrO_3$ solution in DMF was undergone a thorough stirring process followed by sonication of 5 min. $BaZrO_3$ solution was added drop by drop in PVDF solution. More details of sample preparation is reported in our earlier work [38, 39]. Figure 1 shows the different steps followed for the preparation of nanocomposites thin film.

Characterization

The UV–Vis spectra were recorded by Hitachi—4150 spectrophotometer. Aluminium electrodes on thin-film for piezoelectric measurement were prepared by using a vacuum coating unit (Model no, VEQCO Delhi, India). The morphology and phase images were recorded by using SEM–EDX (Model no, MIRA II LMH from TESCAN). The polarization–electric field (P-E) loops were recorded at 100 Hz using the ferroelectric test system (Marine India). Raman spectroscopy was recorded using Renishaw Invia Mirco Raman setup. Differential Scanning Calorimetry (DSC) was recorded using Differential Scanning Calorimetry (DSC); model Q20; (TA Instruments, USA). The d_{33} coefficient of the poled thin film was measured by piezo test (PM100).

Results and discussion

UV–Vis spectra

UV–Vis spectroscopy is an important tool to provide the information on bond structure and optical band gap of materials. The molecular band theory of material describes the promotion of an electron from the ground state (i.e. π, σ, and n- orbits) to higher energy states by absorption of ultraviolet and visible radiation [40].

Figure 2 shows the absorbance of PVDF and PVDF-$BaZrO_3$ nanocomposites with different wavelengths. It

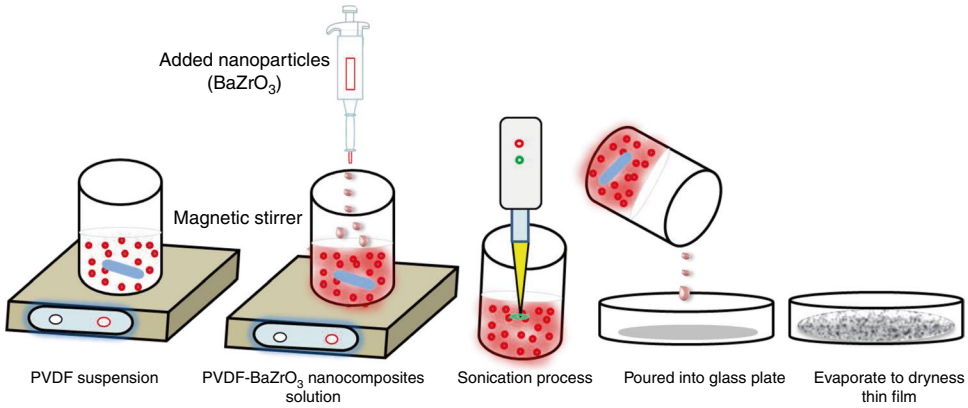

Fig. 1 Preparation of nanocomposites thin film by solution casting method

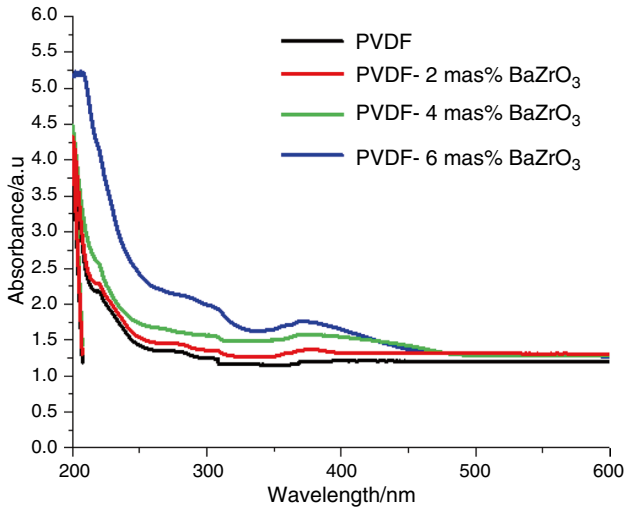

Fig. 2 UV–Vis absorption spectra of **a** PVDF, **b** PVDF-2mass% $BaZrO_3$, **c** PVDF-4mass% $BaZrO_3$, and **d** PVDF -6mass% $BaZrO_3$ nanocomposites

has been observed that the absorbance of PVDF increases with the increasing concentration of $BaZrO_3$ nanoparticles. This may be due to the many defects formed in the chemical structure of PVDF by the addition of $BaZrO_3$. In general, the physical properties of nanoparticles such as particle size, roughness, dispersion, nano-interfaces in polymer affect the absorbance of polymer nanocomposites. The very high absorbance of PVDF nanocomposites in the UV region indicates its interest in UV shielding applications [41].

The absorption edge of PVDF at around 219 nm was shifted to 273, 307 and 366 nm for 2, 4 and 6mass% of $BaZrO_3$ nanoparticles. Generally, in polymer matrix attributed the change in molecular configuration as discussed in literature [42].

Optical band gap E_g was calculated by Tauc,s expression [43, 44]:

$$E = h\nu = \frac{hc}{\lambda} \tag{1}$$

$$(\alpha h\nu)^{m} = B\left(h\nu - E_g\right) \tag{2}$$

where λ represents the maximum wavelength (nm), h is a plank constant, c is the speed of light, α is the absorption coefficient, hν is the photon energy, B is a constant, E_g is the band gap of the material, and the exponent m depends on the type of the transition. The m may be equal to ½ and 2 corresponding to the allowed indirect, allowed direct, forbidden direct, and forbidden indirect transition, respectively [45]. Figure 3a, b shows the variation of $(\alpha h\nu)^{1/2}$ with hν. The band energy gap was calculated by using the method as reported in literature [46, 47].

The direct and indirect optical band gap of PVDF and PVDF nanocomposites are shown in Fig. 3a, b. The direct and indirect optical band gaps of the PVDF- 6mass% $BaZrO_3$ are calculated to be 3.40 and 3.33 eV, respectively. It is comparatively higher than other combinations of $BaZrO_3$ in PVDF. This behavior of PVDF is agreed with our earlier work [48].

PVDF- 6mass% $BaZrO_3$ nanoparticles filled nanocomposites show the highest intensity of UV absorption with maximum width for the absorption window. This can be related to the formation of an interpenetrating network (IPN). This type of network cannot be separated unless chemical bonds are broken. The formation of IPN offers better possibilities for getting extended regions of π^* conjugation, which influences the optical properties significantly.

Raman spectroscopy

Raman spectroscopy is used to sense atomic and molecular motions of organic and inorganic materials at any wavelength except the wavelength of the incident electromagnetic radiation. In polymer nanocomposites, the shift of the Raman line is subjected to the concentration of nanofiller [49, 50].

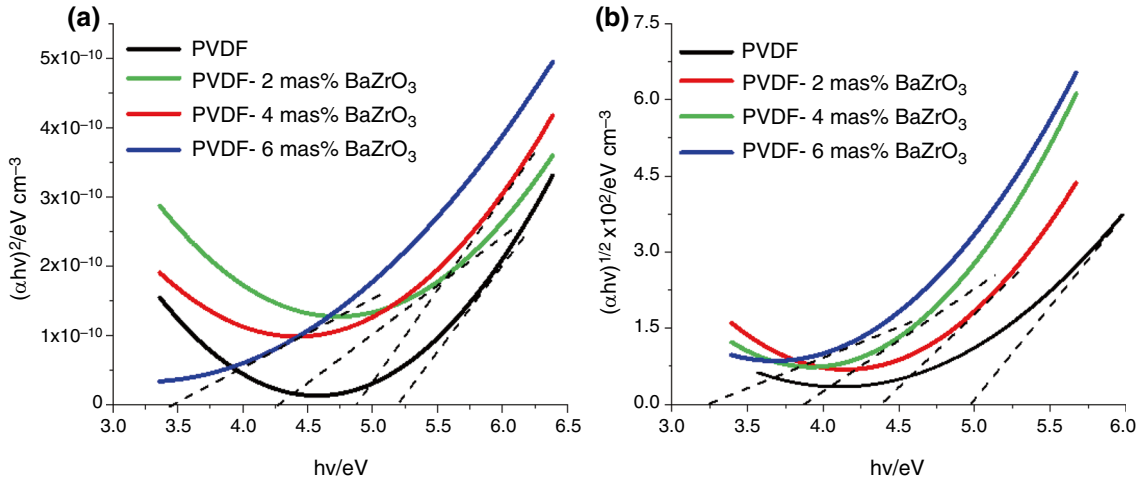

Fig. 3 Plots for **a** Direct optical band gap and **b** Indirect optical band gap for polymer nanocomposite

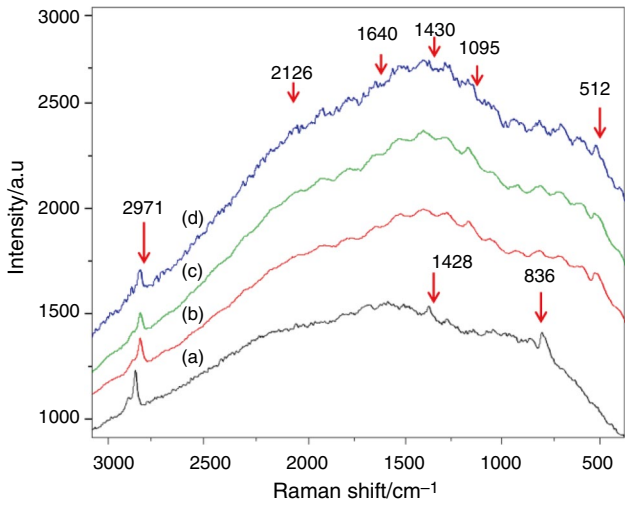

Fig. 4 Micro Raman spectra of **a** PVDF, **b** PVDF-2mass% $BaZrO_3$, **c** PVDF-4mass% $BaZrO_3$, and **d** PVDF -6mass% $BaZrO_3$ nanocomposites

Raman spectra confirm the stretching of the polymer matrix in the presence of nanofiller by means of Raman shift. The Raman shift is related to changes in various vibrations and molecular motions of the polymer-based nanocomposites. The Raman band located at 838 cm^{-1} originates from combined CF_2 bending and CCC skeletal out- of-phase vibrations. It is expected that this band would be sensitive to the loading with $BaZrO_3$ due to skeletal vibrations. Figure 4 shows the Raman spectra in the range of 500 to 3000 cm^{-1} at room temperature with the 532 nm laser line for PVDF and PVDF nanocomposites. In contrast, the PVDF vibration bands exhibited β-phase peaks located at 512, 838, and 1277 cm^{-1} caused by CF_2 vibration. The bands at 512 cm^{-1} attributed to CF_2 bending vibration and higher intensity band at 834 cm^{-1} due to out-of-phase combination of CH_2 rocking and CF_2 stretching mode. The intensity of peak increases with increase in nanoparticles concentration. The shift of Raman spectra of PVDF and nanocomposites with $BaZrO_3$ (i.e. 2, 4 and 6mass%) are shown in Fig. 4b–d. The spectra present from 1542 to 1756 cm^{-1} for G band assigned to the in-plane vibration, from 1334 to 1428 cm^{-1} for D band is activated by the presence of disorder in carbon systems and some Raman bands are located at 2126 to 2971 cm^{-1} called the G' band [51–53]. The assignment of bands in Raman spectra of PVDF and nanocomposites are presented in Table 2. The change in position of Raman band of polymer nanocomposites indicates two domains. First domain is compressive strain and second is the expansion domain. It has been observed that by increasing the concentration of $BaZrO_3$, the position of band shifted downwards, suggesting a positive strain resulted in the crowding of nanofillers above the elastic capabilities of the matrix. The band located at 2980 cm^{-1} is shifted downward for PVDF nanocomposites. This band is connected to crystalline domains of PVDF. This means that the contribution of elongational strain becomes visible. This experimental result suggests that the band recorded at 2988 cm^{-1} is corresponding to the crystalline domain of PVDF. The amorphous phase of PVDF accommodates the nanoparticles. The possible electrostatic interaction of oxygen contents of $BaZrO_3$ and partially charged CH_2 group of PVDF nucleates and form high electroactive β-phase induces polymeric chain to orient in all-trans (TTTT) conformation structure [54–56].

Scanning electron microscopy (SEM)

The SEM micrograph (Fig. 5) of PVDF and PVDF-$BaZrO_3$ nanocomposites provides the information of spherulites and dispersion of $BaZrO_3$ nanoparticles in the polymer matrix.

Table 2 Analysis of different peaks/bands in Raman spectra of PVDF and PVDF-$BaZrO_3$ nanocomposites samples

Samples	Peaks/bands				
	CF_2 modes β-phase in500-950/cm^{-1}	CF_2 Symmetric/ Asymmetric stretch in1000-1300/cm^{-1}	CH_2, D-Band in1300-1500/cm^{-1}	G-Band in1500-1900/cm^{-1}	G′-Band in2000-3000/cm^{-1}
PVDF	512 659 836 915	1004 1107 1191 1277	1339 1430	1642 1740	2545 2969
PVDF-2mass% $BaZrO_3$	728 834	1108 1190	1334 1438 1641	1542, 1743 1862	2116 2969
PVDF-4mass% $BaZrO_3$	834 950	1105 1207	1341, 1431, 1643	1746 1869	2120 2483
PVDF-6mass% $BaZrO_3$	832 838	1000 1033 1206	1326, 1428, 1640	1756 1855	2126 2971

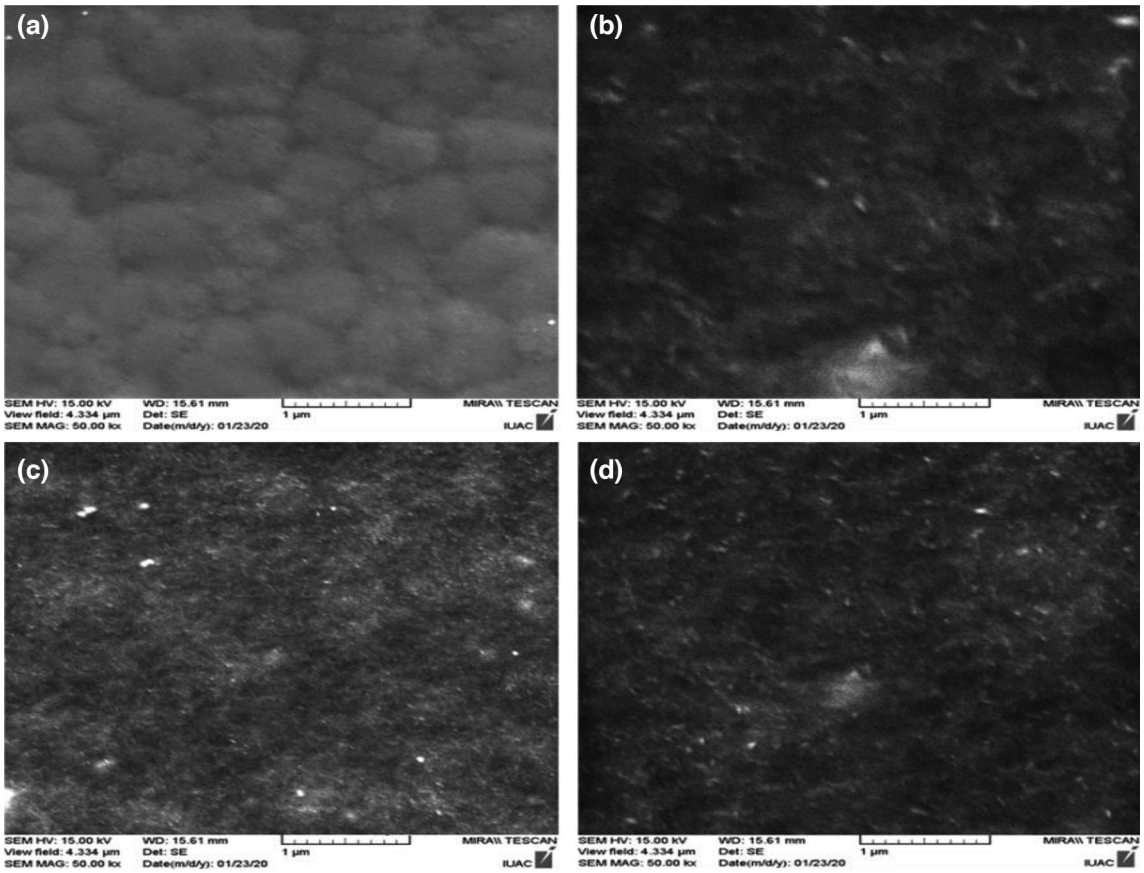

Fig. 5 SEM images of **a** PVDF, **b** PVDF-2mass% $BaZrO_3$, **c** PVDF-4mass% $BaZrO_3$, and **d** PVDF -6mass% $BaZrO_3$ nanocomposites

The SEM image of PVDF shows the well-defined structure of spherulites for which the polymer chains are self-connected into a continuous network along with some scattered pores. The SEM image of nanocomposites reflects that the spherulites are merging with each other and pores are disappearing with increasing concentration of $BaZrO_3$. We could understand from these results that $BaZrO_3$ nanoparticles acted as a nucleation agent leading to close interaction or

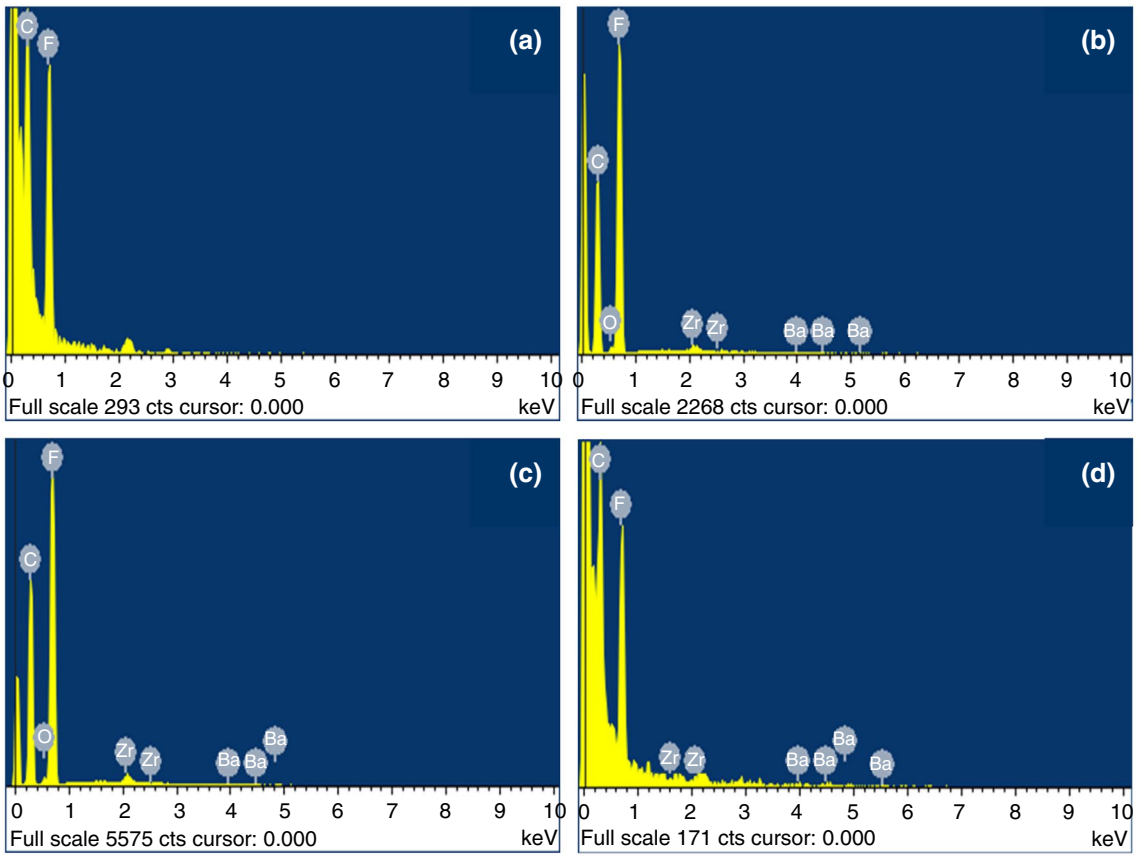

Fig. 6 SEM–EDX spectra of **a** PVDF, **b** PVDF-2mass% $BaZrO_3$, **c** PVDF-4mass% $BaZrO_3$, and **d** PVDF-6mass% $BaZrO_3$ nanocomposites

growth of spherulites in PVDF matrix. The bright spots in PVDF-$BaZrO_3$ nanocomposites show the aggregated region of nanoparticles and the faded part reflects the homogeneous distribution of nanoparticles. The dispersion of nanoparticles is supported by the interaction of oxygen contents of $BaZrO_3$ with the hydrogen bond of PVDF. Also, the surface charge of $BaZrO_3$ nanoparticles helps to smooth the orientation of molecular chain due to the formation of induced dipoles [57, 58]. The formation of nano-crystalline regions of $BaZrO_3$ in PVDF matrix led to a significant improvement in piezoelectric and thermal properties of PVDF.

The EDX spectra (i.e. Figure 6b) are showing the presence of barium, zirconium, oxygen, gold, carbon, and fluorine. The elements Ba, Zr, O, C, and F were originating from the PVDF structure due to the presence of $BaZrO_3$. The presence of gold is due to the coating material of samples was ignored. Each component in nanocomposites samples shows the characteristics peak and peak height is the measurement of percentage concentration of components in PVDF matrix. These results clearly indicate the successful formation of nanocomposites.

Hysteresis *P-E* loops

The charge generation capability of PVDF-$BaZrO_3$ nanocomposites was studied by using polarization–electric field

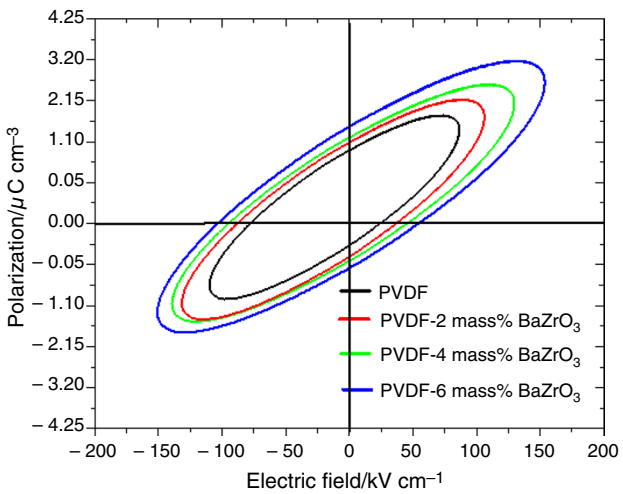

Fig. 7 Electric field dependent polarizations (P–E loop) at 100 Hz for PVDF and PVDF-$BaZrO_3$ nanocomposites at room temperature

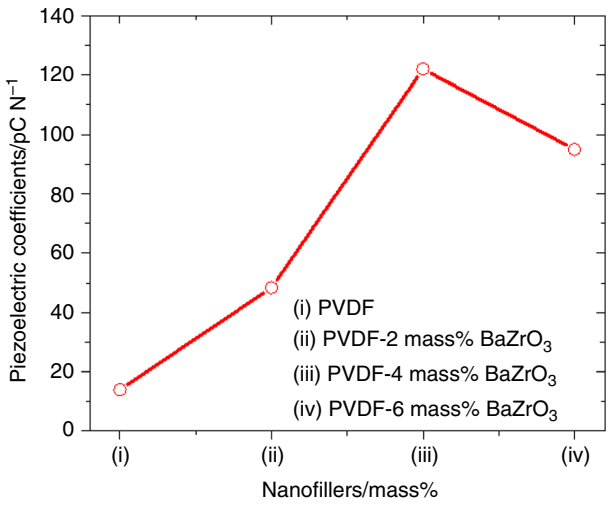

Fig. 8 Piezoelectric coefficient d_{33} for PVDF and PVDF-$BaZrO_3$ nanocomposites at room temperature

(P-E) loop. The P-E loops were recorded for PVDF and PVDF-$BaZrO_3$ nanocomposites with polarization electric field of 200 kV cm^{-1} at room temperature under a frequency of 100 Hz (i.e. Figure 7).

The polarization parameter (i.e. remnant polarization, coercive field, etc.) of PVDF nanocomposites attain a higher value as compared to pure PVDF. For example, the P_r value of PVDF is 1.13 μC cm^{-2}, and P_r value PVDF nanocomposites with 6mass% of $BaZrO_3$ is 3.25 μC cm^{-2}. This change itself demonstrates the enhancement of energy density and dielectric permittivity of PVDF nanocomposites [59]. This is due to the fact that the β-phase is dominated in the structure of PVDF by the addition of $BaZrO_3$. The area of the curve represents the charge storage ability of the material. It could be observed that area of the P-E loop for PVDF nanocomposites is higher than pure PVDF. The P_r value of PVDF nanocomposites attributed charge accumulation at the interface, which facilitates the heterogeneous polarization. The $BaZrO_3$ in PVDF matrix enhances the remnant polarization and coercive field. Therefore, it is reasonable to understand that $BaZrO_3$ nanoparticles are responsible for increasing polarization response as well as charge generation capability of PVDF.

Piezoelectric properties

It is found that d_{33} coefficient of PVDF nanocomposites with 6mass% of $BaZrO_3$ is less than 4mass% of $BaZrO_3$ (Fig. 8). This is due to the fact that the higher concentrations of nanofillers have tendency of agglomeration in polymer matrix leading to poor electrochemical coupling. The modifications of piezoelectric properties are completely caused by the improvement of β-phase in PVDF, which is verified from Raman spectra [38, 59, 60]. The poling field and surface of PVDF are perpendicular to each other during polarization. This arrangement orients the molecular dipoles along the direction of field. This perturbation will dynamically change the position of nuclei and the electrons, which will favor the formation of more and more dipoles. As a result, the opposite facing poles inside the PVDF cancel each other and fixed charges appear on the surface. If V is the applied voltage and d is the thickness of the film. If the thin film is assumed to be behave like a parallel plate capacitor, then d_{33} coefficient will be [61];

$$d_{33} = -\alpha\, CV/F \tag{3}$$

where α is a calibration factor associated with the specimen to be tested. If α is determined a priori via a finite element analysis, C is the capacitance and F is the finite applied force. The capacitance of PVDF nanocomposites enhances many times by the addition of $BaZrO_3$ nanoparticles as reported in our earlier work [38]. This is the origin of increasing piezoelectric coefficients of PVDF.

Differential scanning calorimetry (DSC)

The melting behavior of the polymeric samples and the degree of crystallinity were investigated by differential scanning calorimetry (DSC). Figure 9 shows the DSC of PVDF, PVDF- 2mass% $BaZrO_3$, PVDF- 4mass% $BaZrO_3$, and PVDF- 6mass% $BaZrO_3$ in endothermic mode with the heating rate of 10 °C min^{-1} under the nitrogen medium. Figure 9a–d shows the DSC of β-phase PVDF and nanocomposites with different mass% of $BaZrO_3$. It has been observed that melting temperature (T_m) at 143.04, 140.40, 139.81, and 138.32 °C for PVDF and PVDF nanocomposites samples of different $BaZrO_3$ concentrations.

Figure 9 shows an endothermic peak followed by enthalpy relaxation upon heating. The broad relaxation peak is owing to heating-dependent crystallization. It is noted that the melting peak gives the crystalline and noncrystalline behavior of the material in terms of sharp and broad shape. The enthalpy (ΔH_c) value for nanocomposites is larger as compared to pure samples. That means crystallinity of samples increases in presence of nanofiller. These results are supported by literature [62, 63] and summarized in Table 3. Apart from this, the rearrangement of the molecular chain took place during heating resulting in the shifting of glass transition temperature from amorphous region to crystalline region [64].

The effect of $BaZrO_3$ on glass transition temperature (T_g) can be explained by the enthalpy interaction between the polymer and nanoparticles. The enthalpy of crystallization (ΔH_c) of PVDF increases with increasing concentration of $BaZrO_3$ nanoparticles. Either an increase or decrease in (T_g) can be induced depending on the specific

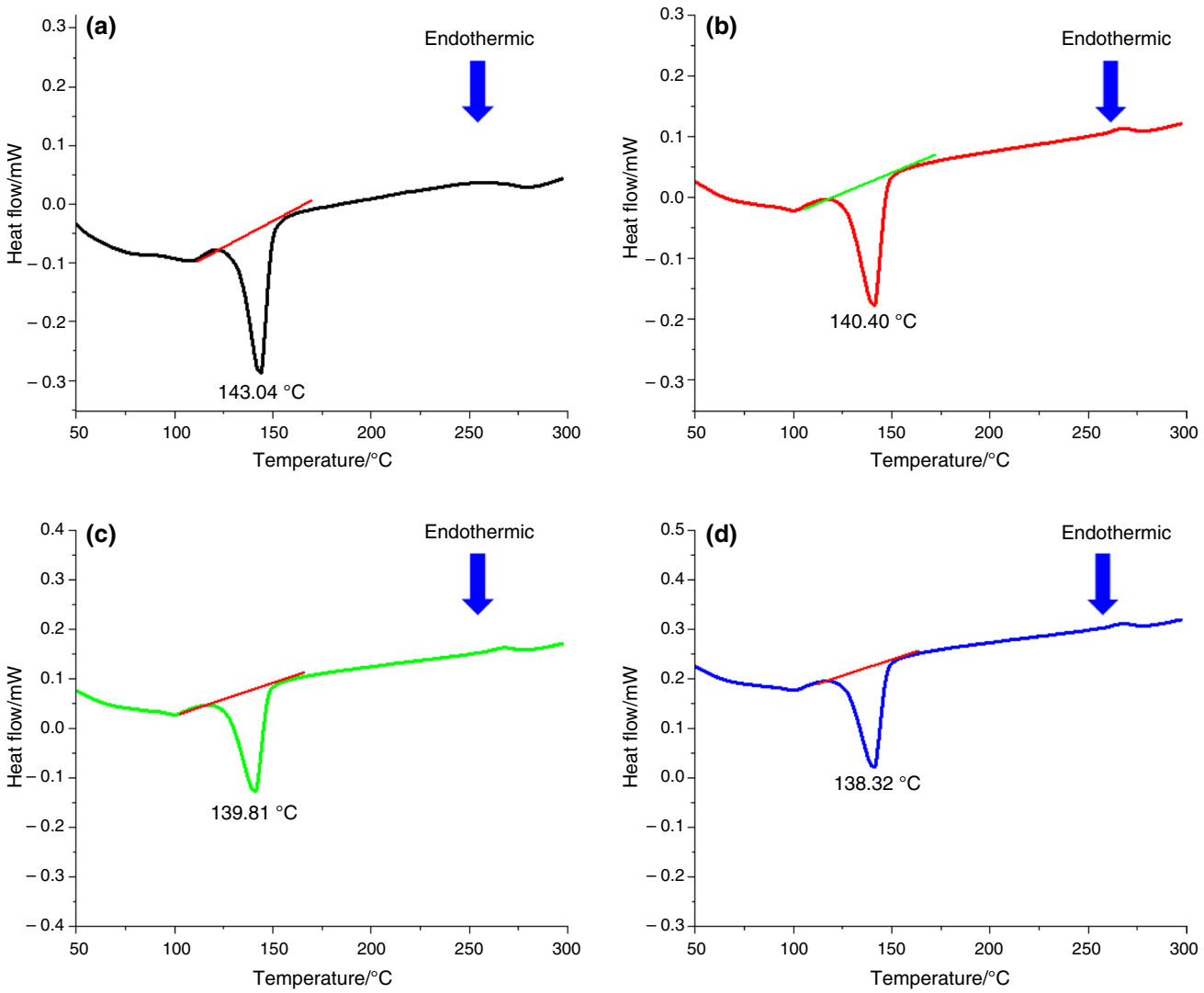

Fig. 9 DSC of **a** PVDF, **b** PVDF-2mass% $BaZrO_3$, **c** PVDF-4mass% $BaZrO_3$, and **d** PVDF-6mass% $BaZrO_3$ nanocomposites

Table 3 DSC parameters of PVDF and PVDF-$BaZrO_3$ nanocomposites samples

Samples	T_m /°C	ΔH_m /J g^{-1}	ΔH_C /J g^{-1}	C_p/J kg^{-1} K^{-1}	X/%
PVDF	143.04	16.59	38.24	1244.55	40.21
PVDF-2mass%$BaZrO_3$	140.40	15.16	40.58	1256.69	45.92
PVDF-4mass%$BaZrO_3$	139.81	12.58	45.71	1332.12	46.58
PVDF-6mass%$BaZrO_3$	138.32	10.44	67.36	1419.56	47.09

T_m, melting temperature, ΔH_m heat of fusion, ΔH_C enthalpy of crystallization, C_p specific capacitance and X, mass fraction crystallinity

capacitance (C_p) interaction [65, 66]. The percentage crystallinity of polymeric samples is based on the mass fraction crystallinity *(X%),* crystallization enthalpy/heat release of crystallization *(ΔH_c)* under DSC scans, which is obtained from the following relations [67–70]:

$$\Delta H_c = kA/M \tag{4}$$

$$X(\%) = \frac{\Delta H_m}{M\Delta H_{100\%,\text{crystalline}}} \times 100\% \tag{5}$$

where k is the instrument constant, which is found to be 1.12; A is the area under the crystallization peak and M is the mass of the sample and $\Delta H_{100\%,\ \text{crystalline}}$ is the heating enthalpy of fusion of pure crystalline PVDF, which is reported to be 104.6 J g^{-1} [71, 72] and ΔH_m melting peak temperature of the polymeric samples. The results are presented in Table 3.

$BaZrO_3$ nanoparticles in PVDF matrix modified the crystalline structure due to the formation of more and more β phases. This means the polymer chain interweaves with nanofillers and forms nucleolus. The polymer nucleation may become a multi-stage process due to the involvement of a wide range of relaxation processes. The $BaZrO_3$ in PVDF matrix modified the crystallization and polarization behavior of PVDF by means of nucleation effect and crystal growth. The possibility of molecular stacking of PVDF molecules cannot ignore. The molecular stacking increases the crystallization rate, and finally, crystallinity. Since the crystallization process is time-dependent, lower cooling rates give the macromolecular chains enough time-to-change conformation. This led to the less energetic arrangement and formation of crystallites at higher temperatures. This mechanism is consistent with the work reported in literature [73, 74].

Conclusions

In addition of $BaZrO_3$ nanoparticles in the PVDF matrix enhances the β-phase by nucleation process. We conclude that electrochemical interaction and nucleation effect in PVDF nanocomposites is the driving force of electroactive and thermal properties. The formation of nanocomposites enhances the charge generation capability and d_{33} coefficient. As a result, the area of the P-E loop increases with the increasing concentration of $BaZrO_3$ nanoparticles. It showed the improvement of piezoelectric properties explores the possible applications in the field of biomedical, robotics, membrane, and sensor. The results of the DSC showed the notable improvements in glass transition temperature, enthalpy, melting point, crystallinity, etc., by incorporation of $BaTiO_3$ nanoparticles in PVDF matrix. The main reason of improvement is the interaction between nanoparticles surfaces and PVDF chains may reform the crystalline structure of PVDF. The enthalpy is considered to support the crystallization and nucleation effect.

Acknowledgements Financial assistance from Aeronautics R&D Board, DRDO New Delhi-110 011 India (Letter no. ARDB/01 l10519021/M/l), is gratefully acknowledged). We are also thankful to Director IUAC, New Delhi for providing characterization facilities. One of the authors Rohan Sagar acknowledges the University Grant Commission (UGC), New Delhi (India) for a providing research fellowship (RGNF-2017-18-SC-UTT-29088).

Declarations

Conflict of interest No potential conflict of interest was reported by the authors.

References

1. Kim M-S, Ahn H-R, Lee S, Kim C, Kim Y-J. A dome-shaped piezoelectric tactile sensor arrays fabricated by an air inflation technique. Sens Actuators A Phys. 2014;212:151–8.
2. Beringer LT, Xu X, Shih W, Shih WH, Schauer CL. Optimization of an electrospun PVDF-TrFe fiber sensor platform for biological applications. Sens Actuators A. 2015;222:293–300.
3. Mei H, Wang R, Feng J, Xia Y, Zhang T. A flexible pressure-sensitive array based on soft substrate. Sens Actuators A. 2015;222:80–6.
4. Cho Y, Park JB, Kim BS, Lee J, Hong WK, Park IK, Jang JE, Sohn JI, Cha S, Kim JM. Enhanced energy harvesting based on surface morphology engineering of P(VDF-TrFE) film. Nano Energy. 2015;16:524–32.
5. Zampetti E, Macagnano A. Flexible piezoelectric transducer based on electrospun PVDF nanofibers for sensing applications. Procedia Eng. 2014;87:1509–12.
6. Bayramol DV, Soin N, Shah T, Siores E, Matsouka D, Vassiliadis S. Energy harvesting smart textiles. Blacksburg: Springer; 2017.
7. Lang C, Fang J, Shao H, Ding X, Lin T. High-sensitivity acoustic sensors from nanofibre webs. Nat Commun. 2016;7:11108.
8. Priya S, Song HC, Zhou Y, Varghese R. A review on piezoelectric energy harvesting: materials, methods, and circuits. J Energy Harvest Syst. 2017;4:3.
9. Chen C, Bai Z, Cao Y, Dong M, Jiang K, Zhou Y. Enhanced piezoelectric performance of $BiCl_3$/PVDF nanofibers-based nanogenerators. Compos Sci Technol. 2020;192:108100.
10. Singh V, Singh B. Fabrication of PVDF-transition metal dichalcogenides based flexible piezoelectric nanogenerator for energy harvesting applications. Mater Today Proc. 2020;28:282–5.
11. Song L, Huang Q, Huang Y, Bi R, Xiao C. An electro-thermal braid-reinforced PVDF hollow fiber membrane for vacuum membrane distillation. J Membr Sci. 2019;591:117359.
12. Al-Osaimi J, Al-Hosiny N, Abdallah S, Badawi A. Characterization of optical, thermal and electrical properties of SWCNTs/PMMA nanocomposite films. Iran Polym J Engl Ed. 2014;23:437–43.
13. Badawi A, Ahmed EM, Mostafa NY, Alomairy SE. Enhancement of the optical and mechanical properties of chitosan using Fe_2O_3 nanoparticles. J Mater Sci Mater Electron. 2017;28:10877–84.
14. Badawi A, Alharthi SS, Mostafa NY, Althobaiti MG, Altalhi T. Effect of carbon quantum dots on the optical and electrical properties of polyvinylidene fluoride polymer for optoelectronic applications. Appl Phys A. 2019;125:858.
15. Indolia AP, Gaur MS. Investigation of structural and thermal characteristics of PVDF/ZnO nanocomposites. J Therm Anal Calorim. 2012;113(2):821–30.
16. Suma GR, Subramani NK, Shilpa KN, Sachhidananda S, Satyanarayana SV. Effect of $Ce_{0\cdot5}Zr_{0.5}O_2$ nano fillers on structural and optical behaviors of poly(vinyl alcohol). J Mater Sci Mater Electron. 2017;28:10707–14.
17. Bai Y, Cheng ZY, Zhang QM. High-dielectric-constant ceramic-powder polymer composites. Appl Phys Lett. 2000;76:3804.
18. Arbatti M, Shan X, Cheng ZY. Ceramic–polymer composites with high dielectric constant. Adv Mater. 2007;19:1369–72.
19. Khatun F, Thakur P, Hoque NA, Kool A, Roy S, Biswas P, Bagchi B, Das S. In situ synthesized electroactive and large dielectric

BaF_2/PVDF nanocomposite film for superior and highly durable self-charged hybrid photo-power cell. Energy Convers Manag. 2018;171:1083–92.
20. Dutta B, Kar E, Bose N, Mukherjee S. Significant enhancement of the electroactive β-phase of PVDF by incorporating hydrothermally synthesized copper oxide nanoparticles. RSC Adv. 2015;5:105422–34.
21. Dutta B, Kar E, Bose N, Mukherjee S. Smart, lightweight, flexible NiO/poly(vinylidene flouride) nanocomposites film with significantly enhanced dielectric, piezoelectric and EMI shielding properties. J Polym Res. 2017;24:220.
22. Yu S, Zheng W, Yu W, Zhang Y, Jiang Q, Zhao Z. Formation mechanism of β- phase in PVDF/CNT composite prepared by the sonication method. Macromolecules. 2009;42:8870–4.
23. Gaur MS, Singh PK, Ali A, Singh R. Thermally stimulated discharge current (TSDC) characteristics in β-phase PVDF–BaTiO3 nanocomposites. J Therm Anal Calorim. 2014;117(3):1407–17.
24. Kar E, Bose N, Das S, Mukherjee N, Mukherjee S. Temperature dependent dielectric properties of self-standing and flexible poly(vinylidene fluoride) films infused with Er^{3+} doped GeO_2 and SiO_2 nanoparticles. J Appl Polym Sci. 2016;133:44016.
25. Mohanty HS, Kumar A, Kulriya PK, Thomas R, Pradhan DK. Dielectric/ferroelectric properties of ferroelectric ceramic dispersed poly (vinylidene fluoride) with enhanced β-phase formation. Mater Chem Phys. 2019;230:221–30.
26. Uchino K. Advanced piezoelectric materials: science and technology. Philadelphia: Wood head Publishing; 2010.
27. Cai E, Liu Q, Zhou S, Zhu Y, Xue A. Structure, piezoelectric, dielectric and ferroelectric properties of lead-free (1–x)($Ba_{0.85}$ $Ca_{0.15}$)($Ti_{0.93}$ $Zr_{0.07}$)O3–x($Bi_{0.5}$ $K_{0.5}$)TiO_3 ceramics. J Alloys Compd. 2017;726:1168–78.
28. Mayeen A, Kala MS, Sunija S, Rouxel D, Bhowmik RN, Thomas S, Kalarikkal N. Flexible dopamine-functionalized $BaTiO_3$/$BaTiZrO_3$/$BaZrO_3$-PVDF ferroelectric nanofibers for electrical energy storage. J Alloys Compd. 2020;837:155492.
29. Huaying L, Hern K. Thermal degradation and kinetic analysis of PVDF/modified MMT nanocomposite membranes. Desalination. 2008;234:9–15.
30. Bertini F, Canetti M, Audisio G, Costa G, Falqui L. Characterization and thermal degradation of propylene-montmorillonite nanocomposites. Polym Degrad Stab. 2006;91:600–5.
31. Dobkowski Z. Thermal analysis techniques for characterization of polymer materials. Polym Degrad Stab. 2006;91:488–93.
32. Lopes A, Costa CM, Tavares C, Neves I, Lanceros MS. Nucleation of the electroactive phase and enhancement of the optical transparency in low filler content poly(vinylidene)/clay nanocomposites. J Phys Chem C. 2011;115:18076–82.
33. Martins P, Lopes A, Lanceros MS. Electroactive phases of poly(vinylidene fluoride): determination, processing and applications. Prog Polym Sci. 2014;39:683–706.
34. Sajkiewicz P, Wasiak A, Gocłowski Z. Phase transitions during stretching of poly(vinylidene fluoride). Eur Polym. 1999;35:423–9.
35. Huang Li X, Yang C, Cheng Y. Thermal reaction properties of aluminum/copper (II) oxide/poly(vinylidene fluoride) nanocomposite. J Therm Anal Calorim. 2015;124(2):899–907.
36. Boccaccio T, Bottino A, Capannelli G, Piaggio P. Characterization of PVDF membranes by vibrational spectroscopy. J Membr Sci. 2002;210:315–29.
37. Imamura R, Silva A, Gregorio R. Phase transformation induced in poly(vinylidene fluoride) by stretching. J Appl Polym Sci. 2008;110:3242–6.
38. Sagar R, Gaur SS, Gaur MS. Effect of $BaZrO_3$ nanoparticles on pyroelectric properties of polyvinylidene fluoride (PVDF). J Ther Anal Calorim. 2016;128:1235–9.
39. Sagar R, Gaur MS, Rogachev AA. Piezoelectric and pyroelectric properties of ceramic nanoparticles-based nanostructured PVDF/PVC blend nanocomposites. J Therm Analys Calorim. 2020. https://doi.org/10.1007/s10973-020-09979-z.
40. Kumar R, Ali SA, Mahur AK, Virk HS, Singh F, Khan SA, Avasthi DK, Prasad R. Study of optical band gap and carbonaceous clusters in swift heavy ion irradiated polymers with UV–vis spectroscopy science direct. Nucl Instrum Meth Phys Res B. 2008;266:1788–92.
41. Kim H, Baik DH, Gyu Y. Structures, electrical, and dielectric properties of PVDF-based nanocomposite films reinforced with neat multi-walled carbon nanotube. Macromol Res. 2012;20:920–7.
42. Guirguis OW, Manel TH. Optical study of poly (vinyl alcohol)/hydroxypropyl methylcellulose blends. J Mater Sci. 2011;46:5775–89.
43. Tsai FC, Chang CC, Liu LC, Chen WC, Jenekhe SA. New thiophene-linked conjugated poly(azomethine)s: theoretical electronic structure. Synthes Prop Macrmol. 2005;38:1958.
44. Baig U, Gondal MA, Ilyas AM, Sanagi MM. Band gap engineered polymeric-inorganic nanocomposite catalysts: synthesis, isothermal stability, photocatalytic activity and photovoltaic performance. J Mater Sci Technol. 2017;33:547–57.
45. Ibrahim S, Ahmad R, Joha MR. Conductivity and optical studies of plasticized solid polymer electrolytes doped with carbon nanotube. J Chemilumi. 2012;132:147–52.
46. Ammar AH, Farag AAM, Abo-Ghazala MS. Influence of Sb addition on the structural and optical characteristics of thermally vacuum evaporated Sb x Se 1–x thin films. J Alloy Compd. 2017;694:752–60.
47. Kumar R, Singh P. UV–visible and infrared spectroscopic studies of Li3+ and C5+ irradiated PADC polymer. Result Phys. 2013;3:122–8.
48. Miodyńska M, Bajorowicz B, Mazierski P, Lisowski W, Klimczuk T, Winiarski MJ. Preparation and photocatalytic properties of $BaZrO_3$ and $SrZrO_3$ modified with Cu_2 O/Bi_2O_3 quantum dots. Solid State Sci. 2017;74:13–23.
49. Anagnostopoulos G, Androulidakis C, Koukaras E, Tsoukleri GN. Stress transfer mechanisms at the submicron level for graphene/polymer systems. Appl Mater Interface. 2015;7:4216–23.
50. Colomban P. Understanding the nano—and macromechanical behaviour, the failure and fatigue mechanisms of advanced and natural polymer fibres by Raman/IR microspectrometry. Adv Nat Sci Nanosci Nanotechnol. 2013;4:13001.
51. Lovinger AJ. Ferroelectric polymers. Science. 1983;220:1115–21.
52. Lando JB, Peterlin A. Nuclear magnetic resonance and x-ray determination of the structure of poly(vinylidene fluoride). J Poly Sci Part A. 1966;4:941–51.
53. Scheinbeim J, Nakafuku C, Pae KD. High-pressure crystallization of poly(vinylidene fluoride). J Appl Phy. 1979;50:4399–405.
54. Chen S, Yao K, Tay FEH, Liow CL. Ferroelectric poly(vinylidene fluoride) thin films on Si substrate with the β phase promoted by hydrated magnesium nitrate. J Appl Phys. 2007;102:104108.
55. Lopes AC, Costa CM, Tavares CJ. Nucleation of the electroactive γ phase and enhancement of the optical transparency in low filler content Poly(vinylidene)/Clay Nanocomposites. J Phys Chem C. 2011;115:18076–82.
56. Gomes J, Nunes JS, Sencadas V. Influence of the β-phase content and degree of crystallinity on the piezo- and ferroelectric properties of poly(vinylidene fluoride). Smart Mater Struct. 2010;19:65010–65010.
57. Rahul N, Somasekhara RT. Self-powered flexible piezoelectric nanogenerator made of poly (vinylidene fluoride)/Zirconium oxide nanocomposites. Mater Res Express. 2019;6:115330.
58. Mohanty HS, Kumar A, Kulriya PK, Thomas R, Pradhan DK. Dielectric/ferroelectric properties of ferroelectric ceramic

dispersed poly (vinylidene fluoride) with enhanced β-phase formation. Mater Chem Phys. 2019;230:221–30.
59. Elashmawi IS, Gaabour L. Raman, morphology and electrical behavior of nanocomposites based on PEO/PVDF with multiwalled carbon nanotubes. Result Phys. 2015;5:105–10.
60. Lederle F, Härter C, Beuermann S. Inducing β phase crystallinity of PVDF homopolymer, blends and block copolymers by antisolvent crystallization. J Fluor Chem. 2020;12:109510–22.
61. Qing G, Cao GZ, Shen Y. Measurements of piezoelectric coefficient d_{33} of lead zirconate titanate thin films using a mini force hammer. J Vib Acoust. 2013;135:011003–11.
62. You Y, Huang X, Pu Z, Jia K, Liu X. Enhanced crystallinity, mechanical and dielectric properties of biphenyl polyarylene ether nitriles by unidirectional hot-stretching. J Polym Res. 2015;22:221.
63. You Y, Wei R, Yang R, Yang W, Hua X, Liu X. Crystallization behaviors of polyarylene ether nitrile filled in multi-walled carbon nanotubes. RSC Adv. 2016;6:70877–83.
64. Du YouY, X, Mao H, Tang X, Wei R, Liu X. Synergistic enhancement ofmechanical, crystalline and dielectric properties of polyarylene ether nitrile-based nanocomposites by unidirectional hot stretching-quenching. Polym Int. 2017;66:1151–8.
65. Agarwal H, Yadav S, Jaiswar G. Effect of nanoclay and barium sulfate nanoparticles on the thermal and morphological properties of polyvinylidene fluoride nanocomposites. J Therm Anal Calorim. 2017;129(3):1471–9.
66. Kao KC. Dielectric phenomena in. Solids1st ed. San Diego: Elsevier Academic Press,; 2004. p. 579.
67. Wang TT, Herbert JM, Glass AM. The applications of ferroelectric polymers. 1st ed. New York: Blackie; 1988.
68. Lines M, Glass A. Principles and applications of ferroelectrics and related materials. Oxford: Oxford Clarendon Press; 1977.
69. Dang DM, Zhou T, Yao SH. Advanced calcium copper titanate/polyimide functional hybrid films with high dielectric permittivity. Adv Mater. 2009;21:2077–82.
70. Prakash BS, Varma KBR. Dielectric behavior of CCTO/epoxy and Al-CCTO/epoxy composites. Compos Sci Tech. 2007;67:2363–8.
71. Srivastava A, Maiti P, Parkash O. Mechanical and dielectric properties of $CaCu_3Ti_4O_{12}$ and La doped $CaCu_3Ti_4O_{12}$ poly(vinylidene fluoride) composites. Compos Sci Tech. 2014;93:83–9.
72. Srivastava A, Jana KK, Parkash O. Mechanical and dielectric behaviour of $CaCu_3Ti_4O_{12}$ and Nb doped $CaCu_3Ti_4O_{12}$ poly(vinylidene fluoride) composites. J Compos. 2014;52:769379–89.
73. Sajkiewicz P, Wasiak A. Phase transitions during stretching of poly (vinylidene fluoride). Eur Polym. 1999;35:423–9.
74. Neidh FM, Beaume F. Structural evolution of PVDF during storage or annealing. Polymer. 2004;45:1679–88.